Letter

Higher-order magnetic anisotropy in soft-hard magnetic materials

Nguyen Thanh Binh [1,*] Sarah Jenkins [1,2,3] Sergiu Ruta [1,4] Richard F. L. Evans [1] and Roy W. Chantrell [1]

[1]*Department of Physics, University of York, York YO10 5DD, United Kingdom*

[2]*TWIST Group, Institut für Physik, Johannes Gutenberg-Universität, 55128 Mainz, Germany*

[3]*TWIST Group, Institut für Physik, University of Duisburg-Essen, 47057 Duisburg, Germany*

[4]*The Department of Engineering and Mathematics, Sheffield Hallam University, Sheffield S1 1WB, United Kingdom*

(Received 14 October 2022; accepted 19 December 2022; published 27 January 2023)

We have computationally studied the properties of higher-order magnetic anisotropy constants in an $L1_0/A1$-FePt core-shell system which is characterized by a strong second-order two-ion Fe-Pt anisotropy component. We show that the core-shell structure induces an unexpected fourth-order anisotropy constant K_2, the magnitude of which varies nonmonotonically with the core-size ratio R reaching a peak at $R \approx 0.50$. Furthermore, we find that K_2 scales with the normalized magnetization by $(M/M_s)^{2.2}$ at temperatures below the Curie temperature, a remarkable deviation from the established Callen-Callen theory which instead predicts a scaling exponent of 10. We construct an analytic model which demonstrates K_2 arises from the canting of the core and shell magnetization, and successfully reproduces and justifies the scaling exponent obtained from numerical simulation.

DOI: 10.1103/PhysRevB.107.L041410

Heat-assisted magnetic recording (HAMR) is emerging as the next-generation approach for magnetic recording [1,2]. The functioning of HAMR requires the writing medium to be made of a magnetic material with high anisotropy and low Curie temperature. FePt in the $L1_0$ phase satisfies this requirement, and thus has been studied extensively for potential HAMR applications [3,4]. As prepared, bulk-alloy FePt generally exists in the $A1$ phase in which Fe and Pt atoms are randomly distributed, thus resulting in a low magnetic anisotropy. However, at high temperatures FePt can undergo a transition to the ordered $L1_0$ phase [5], sketched in Fig. 1. The exceptionally large magnetocrystalline anisotropy of $L1_0$-FePt stems from a hybridzation between the $3d$ Fe and $5d$ Pt orbitals along the [001] crystal direction [6–11] which brings into play the strong spin-orbit coupling of the Pt, resulting in a dominant two-ion anisotropy component [12,13] in addition to the local single-site anisotropy.

Measurements of the second-order anisotropy constant K_1 in bulk $L1_0$-FePt using a simple angular form of the magnetic anisotropy energy function, $E = K_1 \sin^2\theta$, have generally been consistent and well established [12–17], with values for the magnetic anisotropy energy as high as 6.2 MJ/m^3 [17]. On the contrary, a consensus on the existence and the significance of the fourth-order anisotropy constant K_2 is lacking. Previous studies have arrived at conflicting conclusions where K_2 has been argued to be a misinterpretation [17], negligibly small compared to K_1 [16], or non-negligible [12]. In addition, a further issue drawing attention is a reported deviation of the scaling of K_2 [16] from the classical Callen-Callen power law [18] which, interestingly, has also been observed in other materials [19,20].

Furthermore, a recent study by Sepehri-Amin *et al.* [21] on $L1_0$-FePt thin films discovered an effect of Pt enrichment on the film surface regardless of the FePt composition, which subsequently was shown to distort the ordered structure of the $L1_0$ phase and thus reduce the magnetocrystalline anisotropy of the FePt grains. This phenomenon is manifested via a heavy intermixing of Fe atoms and Pt atoms on the grain surface. The proportions of Fe and Pt atoms at various distances from the grain surface are shown to be dependent on grain size. The intermixing between Fe and Pt atoms at the grain surface compromises the chemical ordering of the $L1_0$-FePt grain, thus reducing the uniaxial anisotropy. The impact of this Pt segregation is found to be more pronounced in grains smaller than 15 nm, which is detrimental for HAMR where smaller grain sizes are desired. The varying relative proportion of the two $L1_0/A1$ phases has also been seen to affect the uniaxial magnetic anisotropy in previous experimental studies of phase-graded thin films [22]. The effect of Pt surface segregation in a phase-graded FePt system, therefore, necessitates an investigation into quantifying the impact of $L1_0/A1$ phase composition to the anisotropy of $L1_0$-FePt.

In this Letter we present a computational study using an atomistic model showing the existence of a fourth-order anisotropy component of phase-coupled $L1_0/A1$-FePt core-shell grains which are specifically constructed to replicate the aforementioned Pt surface segregation effect. We propose an analytic model to explain the properties of this fourth-order anisotropy and show that the applicability of our analytic model can be extended to a generic nanocomposite material with soft-hard magnetic interlayers.

We construct elongated FePt grains with faceted surfaces following the method of Moreno *et al.* [23] which closely resemble realistic ones found in a typical HAMR recording medium [21]. The grains are elongated along the [001] lat-

*Corresponding author: btn500@york.ac.uk

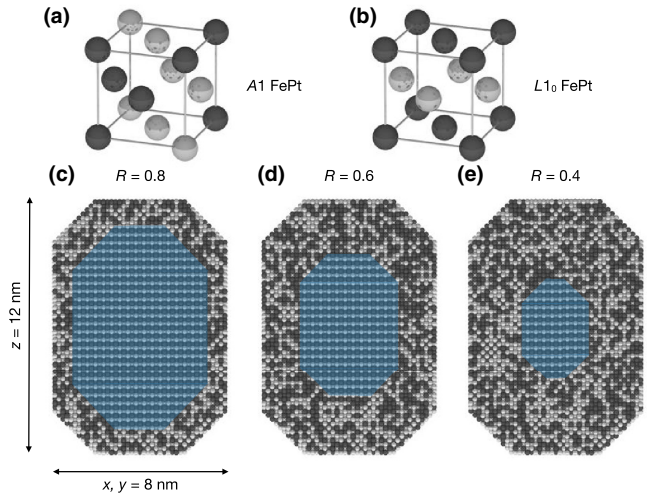

FIG. 1. The crystal structures of FePt: (a) the disordered $A1$-fcc bulk-alloy $Fe_{0.5}Pt_{0.5}$ and (b) ordered $L1_0$-fct. Dark and light spheres indicate Fe and Pt atoms, respectively. Cross-sectional views of the simulated $L1_0/A1$ core-shell grains with core-size ratios (c) $R = 0.80$, (d) $R = 0.60$, and (e) $R = 0.40$ showing different volume fractions of the ordered and disordered phases. The core ordered region in each cross section is indicated by the shaded area.

tice direction by a shape factor of 1.5. In order to replicate the effect of Pt surface segregation, the grains are structured with a core made of the ordered $L1_0$-phase FePt surrounded by a disordered $A1$-phase FePt shell. The grain size is fixed at 8 nm × 8 nm × 12 nm. The diameter of the core can be freely adjusted so as to reproduce varying degrees of ordering through a surface coupling effect between the $L1_0$ and $A1$ phase. The fractional core size R of the grain is defined as $R = d_{\text{shell}}/d_{\text{grain}}$, where d_{core} is the core diameter and d_{grain} the entire grain diameter. In simulations R is varied between 0.05 and 0.95. The lower and upper bounds of R represent two extreme cases: When $R = 0.05$ the $L1_0$ core consists of only one single atom, while when $R = 0.95$ the grain has only one atomistic layer of the $A1$ shell. Cross-sectional views of the core-shell grains with various core sizes R are shown in Fig. 1. The unit cell of the fct $L1_0$-FePt is slightly compressed on the c axis [24–26] while that of the fcc $A1$-FePt is not. For simulation efficiency and without altering any physical properties, a common unit cell is implemented for both phases with a uniform cubic shape and a lattice spacing of $a = 0.3795$ nm obtained from experiments and consistent with previous computational studies [25–28].

Our simulations are carried out using the VAMPIRE atomistic simulation software package [29,30] using a constrained Monte Carlo (CMC) integrator [31]. The system magnetization can be constrained at an angle θ to the easy axis which is oriented along the z direction. At temperatures varying from 0 to 1000 K, a full angular sweep is performed for θ from 0° to 180°. The anisotropy constants are computed via the angular-dependent restoring torque $\partial E(\theta)/\partial\theta$ [31–33]. For a uniaxial system, $E(\theta)$ can be expressed as a power series, $E = E_0 + K_1 \sin^2(\theta) + K_2 \sin^4(\theta) + \cdots$, where the constant E_0 can usually be omitted and K_1 and K_2 are the second- and fourth-order anisotropy constants, respectively. Therefore, by fitting to the torque computed from simulation output, the values of anisotropy constant(s) can be determined.

TABLE I. Core-shell simulation parameters.

Parameter	Notation	Unit	$L1_0$ phase	$A1$ phase
Atomistic spin moment	μ_s	μ_B	3.23	3.23
Local anisotropy	k_{loc}	meV/atom	−0.097	0
Two-ion anisotropy	k_{2ion}	meV/atom	1.427	0
Total exchange [36]	J^0	J/link	3×10^{-21}	3×10^{-21}
CMC equilibration steps			2×10^5	2×10^5
CMC total step			8×10^5	8×10^5

The spin Hamiltonian of the core-shell simulations is the sum of the respective Hamiltonian of the $L1_0$-phase core and of the $A1$-phase shell $\mathscr{H} = \mathscr{H}_{\text{core}} + \mathscr{H}_{\text{shell}}$ which, following the standard Heisenberg form, includes the exchange and anisotropy components without an external magnetic field **B** term. In general the exchange can be written in tensor form $-(\hat{\mathbf{S}}_i)^T \tilde{\mathscr{J}}_{ij} \hat{\mathbf{S}}_j$, where the $\tilde{\mathscr{J}}_{ij}$ encapsulates anisotropic exchange and the Dzyaloshinskii-Moriya interaction. In the case of the $A1$ phase of FePt the exchange is isotropic while for the $L1_0$ phase the exchange is anisotropic and can be expressed [34] as the sum of a diagonal tensor plus a two-ion anisotropy term $\tilde{\mathscr{J}}_{ij} = \mathscr{J}_{ij} + 2\mathscr{K}_{\text{2ion}}$. The Hamiltonian of the core and of the shell are given as follows,

$$\mathscr{H}_{\text{core}} = -\frac{1}{2} \sum_{i,j \in \text{tn}} \hat{\mathbf{S}}_i^T (\mathscr{J}_{ij} + 2\mathscr{K}_{\text{2ion}}) \hat{\mathbf{S}}_j - k_{\text{loc}}^{L1_0} \sum_{i \in \text{tn}} \left(\hat{\mathbf{S}}_i^z\right)^2,$$

$$\mathscr{H}_{\text{shell}} = -\frac{1}{2} \sum_{i,j \in \text{tn}} \hat{\mathbf{S}}_i^T \mathscr{J}_{ij} \hat{\mathbf{S}}_j - k_{\text{loc}}^{A1} \sum_{i \in \text{tn}} \left(\hat{\mathbf{S}}_i^z\right)^2, \quad (1)$$

where $\hat{\mathbf{S}}_i$ and $\hat{\mathbf{S}}_j$ are spin unit vectors, $\mathscr{J}_{ij}$ the (isotropic) exchange energy tensor between pair (i, j) within the truncated-neighbor range tn, and k_{loc}^{A1} and $k_{\text{loc}}^{L1_0}$ the local, in-plane single-site anisotropy of the respective phase, the numerical values of which in simulations are respectively set to 0 [35] and −0.097 meV/atom [34]. Unlike the exchange, the expression for anisotropy does not have to avoid double counting, thus explaining the prefactor 2 of $\mathscr{K}_{\text{2ion}}$ which cancels out the summation prefactor 1/2. In FePt, the exchange interaction $\mathscr{J}_{ij}$ extends further than strictly nearest neighbors. However, since the exchange interaction strength decreases rapidly with increasing distance between neighboring atoms, a reasonably good model includes the exchange interactions truncated after the next-next-nearest neighbors. The calculation of the truncated $\mathscr{J}_{ij}$ and $\mathscr{K}_{\text{2ion}}$ is described in Supplemental Material Sec. S1 [36] which yields a Curie temperature of around 700 K for both ordered and disordered phases, comparable with experiment [37]. Numerical values of exchange energy, anisotropies, and other simulation parameters are tabulated in Table I. Simulations are repeated ten times to compute statistical values.

The magnetocrystalline anisotropy energy, if assumed to include only a second-order anisotropy term $E = K_1 \sin^2(\theta)$, would imply a restoring torque $\tau(\theta) \propto \sin(2\theta)$. However, our simulation results [a sample shown in Fig. 2(a)] demonstrate that a fit (dashed line) to the calculated torque is noticeably skewed from the simulation data (solid symbols). In contrast,

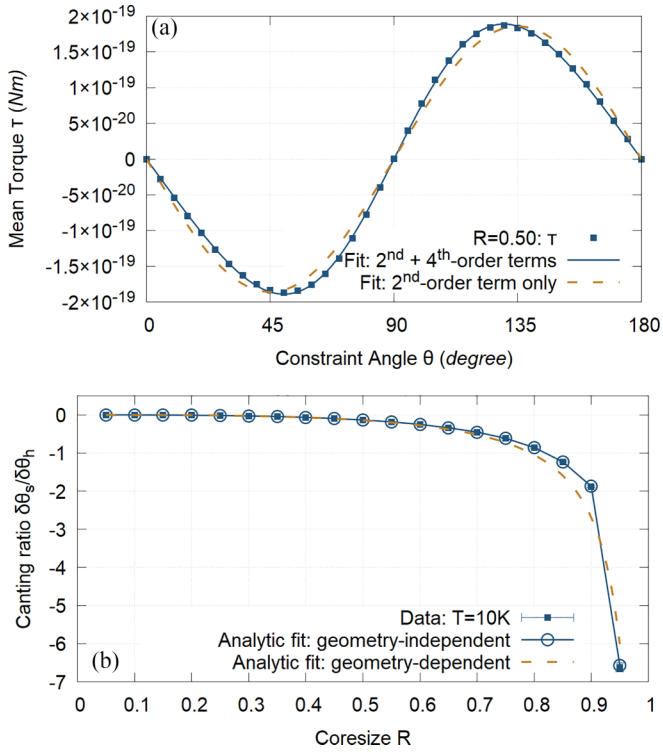

FIG. 2. (a) Fitting to the torque τ for a core size $R = 0.50$ at 10 K displays a clear deviation from simulation data (solid symbols) if including only a second-order anisotropy term (dashed line), but matches better if adding a fourth-order anisotropy term (solid line). (b) The canting of the core and shell magnetization with analytic fits.

when a fourth-order anisotropy term is added, i.e., $E(\theta) = K_1 \sin^2(\theta) + K_2 \sin^4(\theta)$, the new torque fit (solid line) now matches the simulated data extremely well. The discernible skewing of the torque curve in comparison to a simple $\sin(2\theta)$ profile has been observed, without explanation, in a previous experimental study on FePt granular films [38]. In our simulations, however, the skewed torque curves in Fig. 2(a) are a clear indicator of the existence of a significant fourth-order anisotropy component in the core-shell grains.

The magnitude of the temperature-dependent fourth-order anisotropy K_2, expressed via the K_2/K_1 ratio, is found to be dependent on the core size R with a nonmonotonic variation. Low-temperature data in Fig. 3 indicate that the magnitude of K_2 can be significant (exceeding 20% of K_1) if the proportions of the two phases are comparable, or insignificant (just a few percent of K_1) if one phase dominates. This result is intriguing because it essentially recaptures conflicting observations in the literature [12,16]. Additionally, the classical Callen-Callen power law [18] predicts the scaling behavior $K_2 \propto (M/M_s)^{10}$, where (M/M_s) is the magnetization normalized against the saturated magnetization M_s at 0 K. However, our simulation results conclusively contradict this prediction. The inset of Fig. 4 shows an example of K_2 scaling obtained from simulation for $R = 0.70$ from which we find $\beta \approx 2.3$ only. Overall, the scaling exponent β is found to be consistently lower than the Callen-Callen predicted value of 10. The variation of β for K_2 as a function of R (in Fig. 4) generally conforms to

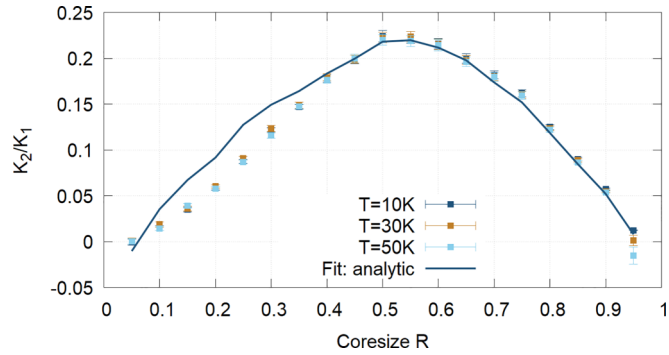

FIG. 3. The dependence of the anisotropy magnitude ratio K_2/K_1 on the core size R. Symbols are the numerically determined values from atomistic simulations and the solid line is the predicted analytic value

$2 \lessapprox \beta \lessapprox 3$ with exceptions seen in the two extreme cases $R = 0.05$ and $R \geqslant 0.80$.

To discuss these two key results, we propose a simple analytic model which we show can explain the origin and behaviors of the fourth-order anisotropy constant K_2 in not only our simulated FePt core-shell system but also a generic material with soft-hard magnetic interlayers. A full description of the analytic model is provided in the Supplemental Material Sec. S2 [36], with the main points outlined as follows. The fundamental observation [illustrated in Fig. 2(b)] is that there exists a canting between the core and shell magnetization which minimizes the total (interlayer exchange and anisotropy) energy of the system. Consider a general core-shell system in which the core is made of a hard-magnetic material having an out-of-plane uniaxial anisotropy k_u (per atom) and the shell a soft-magnetic material with negligible uniaxial anisotropy and, for simplicity, assume coherent magnetization in both core and shell. To minimize the system total magnetic energy E, the constrained angles of the magnetization θ_h and θ_s of the hard- and soft-magnetic phase are allowed to deviate from the overall constraint angle θ by $\delta\theta_h$ and $\delta\theta_s$, respectively, which are sufficiently small to be treated

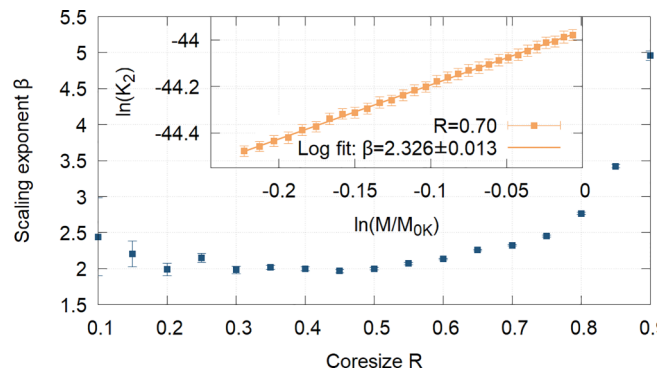

FIG. 4. Variation of the scaling exponent β of the fourth-order anisotropy constant K_2 as a function of the core size R with an inset showing an example of K_2 scaling to the normalized magnetization M/M_s for $R = 0.70$ with a scaling exponent $\beta = 2.326 \pm 0.013$.

as perturbations. Then E can be expressed as

$$E = k_u N_c \sin^2(\theta + \delta\theta_h) - JN_{\text{int}} \cos(\delta\theta_h - \delta\theta_s), \quad (2)$$

where N_c and N_{int} are the number of spins in the core and the core/shell interface, respectively, and J the exchange integral. The first term in Eq. (2) is an anisotropy term and the second an interlayer exchange term which describes the exchange coupling between the core spins and the shell spins. Since θ_h and θ_s are the averaged contributions of all spins in each respective phase, their proportional sum must result in the system θ. Hence, Eq. (2) must be minimized subject to

$$f \cos\theta_h + (1 - f)\cos\theta_s - \cos\theta = 0, \quad (3)$$

where $f = N_c/N_{\text{tot}}$ is the fractional volume of the hard phase with N_{tot} being the total number of spins in the system. Note that for regular geometries, the geometry-independent variables N_c, N_{int}, and N_{tot} can be replaced by the core volume V_c, the interface area A_{cs}, and the total volume V_{tot}, respectively. Substitute $\theta_h = \theta + \delta\theta_h$ and $\theta_s = \theta + \delta\theta_s$ into Eq. (3) and solve to first-order approximation:

$$\delta\theta_s = -\frac{f}{1-f}\delta\theta_h = -\frac{N_c/N_{\text{tot}}}{1 - N_c/N_{\text{tot}}}\delta\theta_h. \quad (4)$$

Analytic fits following from Eq. (4) for both the geometry-dependent case $f = V_c/V_{\text{tot}}$ and the geometry-independent case $f = N_c/N_{\text{tot}}$ are shown in Fig. 2(b). Because of the faceted shape of the simulated core-shell system, the geometry-dependent fit is seen to deviate from simulation data from $R \approx 0.75$ while the geometry-independent fit matches the entire data range extremely well. Minimizing Eq. (2) subject to the constraint Eq. (3) leads to an expression of E which explicitly includes both a second-order and a fourth-order anisotropy term, the magnitude ratio of which is given by

$$\frac{K_2}{K_1} \approx \frac{2k_u N_c}{JN_{\text{int}}}\left(1 - \frac{N_c}{N_{\text{tot}}}\right)^2. \quad (5)$$

To expand the model, consider cases similar to the simulated core-shell FePt in which the dominant part of the core uniaxial anisotropy k_u comes from a two-ion anisotropy. This necessitates two further considerations. First, the two-ion anisotropy is lost on the core/shell interface because of the loss of Pt neighbors from the next-immediate atomistic layer of the shell. Second, when the core is small, the in-plane anisotropy becomes dominant because of vanishing two-ion anisotropy at the core surface. Taking the simulated core-shell FePt as an example, the in-plane anisotropy is the sum of the local single-site anisotropies of the $L1_0$ and $A1$ phase, i.e., $k_{\text{ip}} = k_{\text{loc}}^{L1_0} + k_{\text{loc}}^{A1} = -0.097$ meV/atom, and manifests in the extreme case $R = 0.05$ in Fig. 3 from which K_2/K_1 is seen to become negative. Incorporating these two extra considerations into the first term of Eq. (2) transforms its prefactor $k_u N_c$ to $[k_u(N_c - N_{\text{int}}) + k_{\text{ip}} N_c]$, which subsequently modifies the expression in Eq. (5) to

$$\frac{K_2}{K_1} \approx \frac{2k_u N_c}{JN_{\text{int}}}\left(1 - \frac{N_{\text{int}}}{N_c} + \frac{k_{\text{ip}}}{k_u}\right)\left(1 - \frac{N_c}{N_{\text{tot}}}\right)^2. \quad (6)$$

Figure 3 shows the variation of K_2/K_1 with R at low temperatures in which analytic predictions (solid line) are compared with simulation data (symbols). Both analytic and numerical variations share a similar nonmonotonic form with a peak attained at $R \approx 0.55$. The agreement for $R \geqslant 0.5$ is extremely good, while for $R < 0.5$ the K_2/K_1 values appear to be slightly overestimated by the analytic model. Nonetheless the overall agreement is highly satisfactory, which supports the hypothesis that the fourth-order anisotropy arises from the core/shell spin canting and the exchange energy contribution at the core/shell interface.

Furthermore, the scaling exponent $2 \lessapprox \beta \lessapprox 3$ of K_2 to M/M_s as shown in Fig. 4 can now be explained. Our analytic model finds that $K_2 \propto (k_u)^2/J$ (with a detailed derivation given in the Supplemental Material Sec. S2 [36]). It has been established for $L1_0$-FePt that $k_u \propto (M/M_s)^{2.1}$ [34,39–44] and $J \propto (M/M_s)^2$ via mean-field calculations [45,46]. The resulting scaling, therefore, reads $K_2 \propto (M/M_s)^{2.2}$, thus reproducing $\beta \approx 2.2$ in good agreement with simulation results. Finally, deviations from the analytic model for the two extreme cases $R = 0.05$ and $R \geqslant 0.80$ can be explained from the previously mentioned inherent nature of the grain structure in the respective cases. In the $R = 0.05$ case, the $L1_0$ core is so small that it consists of a single Fe atom which means the two-ion anisotropy component of the $L1_0$ phase completely vanishes, leaving the core with just the negative in-plane single-site Fe anisotropy. This explains the negative ratio K_2/K_1 at $R = 0.05$ as seen in Fig. 3. Meanwhile, for the $R \geqslant 0.80$ case, the $A1$ shell is so thin that it has exactly one or two atomistic layers, hence invalidating the fundamental premise of the analytic calculations which assumes interactions up to the next-next-nearest neighbors. Hence, β of the $R \geqslant 0.80$ case was seen in Fig. 4 to increase exponentially in the $\beta \gtrapprox 3$ range, albeit still significantly lower than the Callen-Callen's predicted value of 10.

In summary, we have presented a comprehensive study of higher-order anisotropy in a phase-coupled $L1_0/A1$-FePt core-shell system. A fourth-order anisotropy is found to exist due to a combination of the canting of the core and shell magnetization and the exchange coupling at the core/shell interface. This fourth-order anisotropy is demonstrated to exhibit a strong dependence on the system geometry and scale with $(M/M_s)^{2.2}$, which does not conform with the Callen-Callen power law. We formulate an analytic model to explain the origin and behaviors of this different fourth-order anisotropy from which a high level of agreement with numerical simulation is achieved. Overall, our findings provide substantial insights into a topic that has otherwise been lacking attention. Because anisotropy decides thermal stability of the writing medium, the significance of fourth-order anisotropy of $L1_0$-FePt can potentially translate to an issue of consideration for HAMR-related applications. Although investigated in the particular case of an $L1_0$/A1-FePt core-shell structure, the analytic model presented is valid for any combination of soft-hard materials. The phenomenon should therefore be observable in a wide variety of systems.

The authors would like to thank Daniel Meilak for assistance with optimizing the simulated core-shell system. The financial support of the Advanced Storage Research Consortium (ASRC) is gratefully acknowledged. S.R. acknowledges funding from the EPSRC TERASWITCH project (project ID EP/T027916/1). S.J. acknowledges funding by the

German Research Foundation (DFG) project No. 320163632. We are also grateful for computational support from the University of York High Performance Computing service, Viking, and the Research Computing team.

[1] R. Rottmayer, S. Batra, D. Buechel, W. Challener, J. Hohlfeld, Y. Kubota, L. Li, B. Lu, C. Mihalcea, K. Mountfield, K. Pelhos, C. Peng, T. Rausch, M. Seigler, D. Weller, and X.-M. Yang, Heat-assisted magnetic recording, IEEE Trans. Magn. **42**, 2417 (2006).

[2] T. McDaniel, Ultimate limits to thermally assisted magnetic recording, J. Phys.: Condens. Matter **17**, R315 (2005).

[3] D. Weller, G. Parker, O. Mosendz, A. Lyberatos, D. Mitin, N. Schmidt, and M. Albrecht, Review article: FePt heat assisted magnetic recording media, J. Vac. Sci. Technol. B **34**, 060801 (2016).

[4] M. H. Kryder, E. C. Gage, T. W. McDaniel, W. A. Challener, R. E. Rottmayer, G. Ju, Y. Hsia, and M. F. Erden, Heat assisted magnetic recording, Proc. IEEE **96**, 1810 (2008).

[5] M. Nakaya, M. Kanehara, M. Yamauchi, H. Kitagawa, and T. Teranishi, Hydrogen-induced crystal structural transformation of FePt nanoparticles at low temperature, J. Phys. Chem. C **111**, 7231 (2007).

[6] G. H. O. Daalderop, P. J. Kelly, and M. F. H. Schuurmans, Magnetocrystalline anisotropy and orbital moments in transition-metal compounds, Phys. Rev. B **44**, 12054 (1991).

[7] A. Sakuma, First principle calculation of the magnetocrystalline anisotropy energy of FePt and CoPt ordered alloys, J. Phys. Soc. Jpn. **63**, 3053 (1994).

[8] P. Oppeneer, Magneto-optical spectroscopy in the valence-band energy regime: Relationship to the magnetocrystalline anisotropy, J. Magn. Magn. Mater. **188**, 275 (1998).

[9] P. Ravindran, A. Kjekshus, H. Fjellvåg, P. James, L. Nordström, B. Johansson, and O. Eriksson, Large magnetocrystalline anisotropy in bilayer transition metal phases from first-principles full-potential calculations, Phys. Rev. B **63**, 144409 (2001).

[10] A. B. Shick and O. N. Mryasov, Coulomb correlations and magnetic anisotropy in ordered $L1_0$ CoPt and FePt alloys, Phys. Rev. B **67**, 172407 (2003).

[11] I. V. Solovyev, P. H. Dederichs, and I. Mertig, Origin of orbital magnetization and magnetocrystalline anisotropy in TX ordered alloys (where T = Fe, Co and X = Pd, Pt), Phys. Rev. B **52**, 13419 (1995).

[12] S. Okamoto, N. Kikuchi, O. Kitakami, T. Miyazaki, Y. Shimada, and K. Fukamichi, Chemical-order-dependent magnetic anisotropy and exchange stiffness constant of FePt (001) epitaxial films, Phys. Rev. B **66**, 024413 (2002).

[13] D. Weller, A. Moser, L. Folks, M. Best, W. Lee, M. Toney, M. Schwickert, J.-U. Thiele, and M. Doerner, High Ku materials approach to 100 Gbits/in.^{2}, IEEE Trans. Magn. **36**, 10 (2000).

[14] T. Bublat and D. Goll, Temperature dependence of the magnetic properties of $L1_0$-FePt nanostructures and films, J. Appl. Phys. **108**, 113910 (2010).

[15] T. Shima, K. Takanashi, Y. K. Takahashi, and K. Hono, Coercivity exceeding 100 kOe in epitaxially grown FePt sputtered films, Appl. Phys. Lett. **85**, 2571 (2004).

[16] K. Inoue, H. Shima, A. Fujita, K. Ishida, K. Oikawa, and K. Fukamichi, Temperature dependence of magnetocrystalline anisotropy constants in the single variant state of $L1_0$-type FePt bulk single crystal, Appl. Phys. Lett. **88**, 102503 (2006).

[17] H. J. Richter, O. Hellwig, S. Florez, C. Brombacher, and M. Albrecht, Anisotropy measurements of FePt thin films, J. Appl. Phys. **109**, 07B713 (2011).

[18] H. Callen and E. Callen, The present status of the temperature dependence of magnetocrystalline anisotropy, and the $l(l+1)/2$ power law, J. Phys. Chem. Solids **27**, 1271 (1966).

[19] B. K. Chatterjee, C. K. Ghosh, and K. K. Chattopadhyay, Temperature dependence of magnetization and anisotropy in uniaxial $NiFe_2O_4$ nanomagnets: Deviation from the Callen-Callen power law, J. Appl. Phys. **116**, 153904 (2014).

[20] D. Miura and A. Sakuma, Power law analysis for temperature dependence of magnetocrystalline anisotropy constants of $Nd_2Fe_{14}B$ magnets, AIP Adv. **8**, 075114 (2018).

[21] H. Sepehri-Amin, H. Iwama, G. Hrkac, K. Butler, T. Shima, and K. Hono, Pt surface segregation in $L1_0$-FePt nano-grains, Scr. Mater. **135**, 88 (2017).

[22] G. Barucca, T. Speliotis, G. Giannopoulos, D. Niarchos, B. Rutkowski, A. Czyrska-Filemonowicz, E. Agostinelli, S. Laureti, A. Testa, and G. Varvaro, Magnetic anisotropy phase-graded $A1/L1_0$-FePt films on amorphous glass substrates, Mater. Des. **123**, 147 (2017).

[23] R. Moreno, S. Poyser, D. Meilak, A. Meo, S. Jenkins, V. K. Lazarov, G. Vallejo-Fernandez, S. Majetich, and R. F. L. Evans, The role of faceting and elongation on the magnetic anisotropy of magnetite Fe_3O_4 nanocrystals, Sci. Rep. **10**, 2722 (2020).

[24] A. Kabir, J. Hu, V. Turkowski, R. Wu, R. Camley, and T. S. Rahman, Effect of structure on the magnetic anisotropy of $L1_0$-FePt nanoparticles, Phys. Rev. B **92**, 054424 (2015).

[25] J. Lyubina, O. Isnard, O. Gutfleisch, K.-H. Müller, and L. Schultz, Ordering of nanocrystalline Fe–Pt alloys studied by *in situ* neutron powder diffraction, J. Appl. Phys. **100**, 094308 (2006).

[26] T. J. Klemmer, N. Shukla, C. Liu, X. W. Wu, E. B. Svedberg, O. Mryasov, R. W. Chantrell, D. Weller, M. Tanase, and D. E. Laughlin, Structural studies of $L1_0$ FePt nanoparticles, Appl. Phys. Lett. **81**, 2220 (2002).

[27] H. Loc Nguyen, L. E. M. Howard, G. W. Stinton, S. R. Giblin, B. Tanner, I. Terry, A. K. Hughes, I. M. Ross, A. Serres, and J. S. O. Evans, Synthesis of size-controlled fcc and fct FePt nanoparticles, Chem. Mater. **18**, 6414 (2006).

[28] S. Aksornniem, R. Evans, R. Chantrell, and R. Silapunt, Magnetic switching in BPM, TEAMR, and modified TEAMR by using dielectric underlayer media, IEEE Trans. Magn. **52**, 1 (2015).

[29] VAMPIRE software package v5 available from https://vampire.york.ac.uk/ (2020).

[30] R. F. L. Evans, W. J. Fan, P. Chureemart, T. A. Ostler, M. O. A. Ellis, and R. W. Chantrell, Atomistic spin model simulations of magnetic nanomaterials, J. Phys.: Condens. Matter **26**, 103202 (2014).

[31] P. Asselin, R. F. L. Evans, J. Barker, R. W. Chantrell, R. Yanes, O. Chubykalo-Fesenko, D. Hinzke, and U. Nowak, Constrained Monte Carlo method and calculation of the temperature dependence of magnetic anisotropy, Phys. Rev. B **82**, 054415 (2010).

[32] X. Wang, R. Wu, D.-s. Wang, and A. J. Freeman, Torque method for the theoretical determination of magnetocrystalline anisotropy, Phys. Rev. B **54**, 61 (1996).

[33] R. Wu and A. Freeman, Spin–orbit induced magnetic phenomena in bulk metals and their surfaces and interfaces, J. Magn. Magn. Mater. **200**, 498 (1999).

[34] O. N. Mryasov, U. Nowak, K. Y. Guslienko, and R. W. Chantrell, Temperature-dependent magnetic properties of FePt: Effective spin Hamiltonian model, Europhys. Lett. **69**, 805 (2005).

[35] P. Schaaf, K. Zhang, C. Lange, A. Holz, M. Weisheit, and S. Faehler, Structure and anisotropy of epitaxial fcc FePt films, Appl. Surf. Sci. **253**, 8107 (2007).

[36] See Supplemental Material at http://link.aps.org/supplemental/10.1103/PhysRevB.107.L041410 for the calculation of the truncated exchange and two-ion anisotropy, and a full description of the analytic model..

[37] O. Hovorka, S. Devos, Q. Coopman, W. J. Fan, C. J. Aas, R. F. L. Evans, X. Chen, G. Ju, and R. W. Chantrell, The Curie temperature distribution of FePt granular magnetic recording media, Appl. Phys. Lett. **101**, 052406 (2012).

[38] T. Saito, K. K. Tham, R. Kushibiki, T. Ogawa, and S. Saito, Separate quantitative evaluation of degree of order and perpendicular magnetic anisotropy for disorder and order portion in FePt granular films, AIP Adv. **11**, 015310 (2021).

[39] R. Skomski, O. N. Mryasov, J. Zhou, and D. J. Sellmyer, Finite-temperature anisotropy of magnetic alloys, J. Appl. Phys. **99**, 08E916 (2006).

[40] R. Skomski, A. Kashyap, and J. Zhou, Atomic and micromagnetic aspects of $L1_0$ magnetism, Scr. Mater. **53**, 389 (2005).

[41] R. Skomski, A. Kashyap, and D. Sellmyer, Finite-temperature anisotropy of PtCo magnets, IEEE Trans. Magn. **39**, 2917 (2003).

[42] J. B. Staunton, S. Ostanin, S. S. A. Razee, B. L. Gyorffy, L. Szunyogh, B. Ginatempo, and E. Bruno, Temperature Dependent Magnetic Anisotropy in Metallic Magnets from an *Ab Initio* Electronic Structure Theory: $L1_0$-Ordered FePt, Phys. Rev. Lett. **93**, 257204 (2004).

[43] J.-U. Thiele, K. R. Coffey, M. F. Toney, J. A. Hedstrom, and A. J. Kellock, Temperature dependent magnetic properties of highly chemically ordered $Fe_{55-x}Ni_xPt_{45}L1_0$ films, J. Appl. Phys. **91**, 6595 (2002).

[44] R. F. L. Evans, L. Rózsa, S. Jenkins, and U. Atxitia, Temperature scaling of two-ion anisotropy in pure and mixed anisotropy systems, Phys. Rev. B **102**, 020412(R) (2020).

[45] U. Atxitia, D. Hinzke, O. Chubykalo-Fesenko, U. Nowak, H. Kachkachi, O. N. Mryasov, R. F. Evans, and R. W. Chantrell, Multiscale modeling of magnetic materials: Temperature dependence of the exchange stiffness, Phys. Rev. B **82**, 134440 (2010).

[46] U. Atxitia, O. Chubykalo-Fesenko, N. Kazantseva, D. Hinzke, U. Nowak, and R. W. Chantrell, Micromagnetic modeling of laser-induced magnetization dynamics using the Landau-Lifshitz-Bloch equation, Appl. Phys. Lett. **91**, 232507 (2007).